

Nanoscale

Accepted Manuscript



This is an *Accepted Manuscript*, which has been through the Royal Society of Chemistry peer review process and has been accepted for publication.

Accepted Manuscripts are published online shortly after acceptance, before technical editing, formatting and proof reading. Using this free service, authors can make their results available to the community, in citable form, before we publish the edited article. We will replace this *Accepted Manuscript* with the edited and formatted *Advance Article* as soon as it is available.

You can find more information about *Accepted Manuscripts* in the [Information for Authors](#).

Please note that technical editing may introduce minor changes to the text and/or graphics, which may alter content. The journal's standard [Terms & Conditions](#) and the [Ethical guidelines](#) still apply. In no event shall the Royal Society of Chemistry be held responsible for any errors or omissions in this *Accepted Manuscript* or any consequences arising from the use of any information it contains.

ARTICLE

Experimental phase diagram of negatively supercoiled DNA measured by magnetic tweezers and fluorescence

Cite this: DOI: 10.1039/x0xx00000x

Received 00th January 2012,
Accepted 00th January 2012

DOI: 10.1039/x0xx00000x

www.rsc.org/Rifka Vlijm^{a,*}, Alireza Mashaghi^{a,*}, Stéphanie Bernard^b, Mauro Modesti^b and Cees Dekker^{a,**}

The most common form of DNA is the well-known B-structure of double-helix DNA. Many processes in the cell, however, exert force and torque, inducing structural changes to the DNA that are vital to biological function. Virtually all DNA in cells is in a state of negative supercoiling, with a DNA structure that is complex. Using magnetic tweezers combined with fluorescence imaging, we here study DNA structure as a function of negative supercoiling at the single-molecule level. We classify DNA phases based on DNA length as a function of supercoiling, down to a very high negative supercoiling density σ of -2.5, and forces up to 4.5pN. We characterize plectonemes using fluorescence imaging. DNA bubbles are visualized by the binding of fluorescently labelled RPA, a eukaryotic single-strand-binding protein. The presence of Z-DNA, a left-handed form of DNA, is probed by the binding of *Za77*, the minimal binding domain of a Z-DNA-binding protein. Without supercoiling, DNA is in the relaxed B-form. Upon going toward negative supercoiling, plectonemic B-DNA is being formed below 0.6pN. At higher forces and supercoiling densities down to about -1.9, a mixed state occurs with plectonemes, multiple bubbles and left-handed L-DNA. Around $\sigma=-1.9$, a buckling transition occurs after which the DNA end-to-end length linearly decreases when applying more negative turns, into a state that we interpret as plectonemic L-DNA. By measuring DNA length, *Za77* binding, plectoneme and ssDNA visualisation, we thus have mapped the co-existence of many DNA structures and experimentally determined the DNA phase diagram at (extreme) negative supercoiling.

Introduction

In the absence of stretching force and torque and under physiological salt conditions, DNA adopts the famous B-form¹ where the backbones exhibit a right-handed helical twist of 10.4 base pairs (bp) per turn. However, many processes in the cell alter the DNA conformation²⁻⁶. Take, for example, DNA transcription: here, the transcription machinery opens up the DNA locally, forming a DNA bubble, and subsequently overwinding the DNA ahead of the transcription site and underwinding the DNA behind it⁵. This over/(under)winding of the DNA induces positive (negative) supercoiled loops, called plectonemes. Beyond protein-binding-induced conformational changes, a complex interplay between applied stretching force and torque, DNA sequence and other factors like temperature and salt conditions determine the local DNA conformation⁷⁻⁹.

Supercoiling is the overwinding (underwinding) of DNA under the influence of positive (negative) torque. For overwound

(underwound) DNA, the number of base pairs per turn becomes larger (smaller) than 10.4 (see Figure 1). At a certain point, the introduction of more turns into the DNA will not change the twisting of the backbones any further, but instead, the DNA forms a supercoiled loop (plectoneme) (Figure 1). The sum of twist in the backbones and number of loops in the DNA (called writhe) is the linking number L_k . For a DNA molecule of which the ends are not free to rotate (i.e., it is topologically constrained), twist ($L_{k,t}$) and writhe ($L_{k,w}$) are interchangeable, and the total linking number $L_k = L_{k,t} + L_{k,w}$ is conserved. Under negative torque, an additional phenomenon can occur where the helix locally opens up into a DNA bubble, exposing two non-hybridized single strands¹⁰. Increased temperature and stretching force promote bubble formation. Certain sequences also do so, such as the transcription initiation TATA-box at promoter sites. The base pairs can even re-stack into a left-handed helix, forming Z-DNA, which has 12 bp per left-handed helical twist¹¹⁻¹³. Understanding the physical properties of

DNA provides the groundwork for a better understanding of the complex function of important processes within the cell¹⁴⁻¹⁶. Although negative supercoiling is ubiquitous in cellular DNA, it remains unclear what conformational state(s) DNA adopts under negative supercoiling.

In the past two decades, a lot of effort was carried out to decipher the many structures of DNA in various regimes of force and linking number, both experimentally and theoretically. First S (stretched) DNA was discovered by measuring the extension over a wide force range. Around 65pN the extension of a rotationally unconstrained (nicked) molecule increased significantly, which was interpreted as converting B-DNA to S-DNA^{17, 18}. From these measurements S-DNA was estimated to have a contour length 1.7 times as long as B-DNA with a helix repeat of 35bp per turn^{19, 20}. Driven by the discovery of S-DNA, more experiments of this type were performed and the structural states, B-, S-, P-, supercoiled (sc-)P, melted and L/Z-DNA were described^{4, 19-28}. Here P is highly overwound DNA, with a base-pair repeat of ~3bp and an extension 1.7 times as long as B-DNA, hypothesized to have the sugar-phosphate backbone in the middle with the unpaired bases exposed (hence the name 'P-DNA' after the early model of Pauling). Experiments have recently been conducted to examine the states of underwound DNA. Under moderate forces (~10pN), and very strong underwinding, the melted DNA has been suggested to assume a left-handed structure as opposed to an open bubble conformation²⁹. The force and supercoiling density at which state transitions occurred appeared to be sequence dependent³⁰. Several names have been used for this left-handed DNA. The most well-known one is Z-DNA, which is well characterized and for which the crystal structure is known^{11-13, 31}. It has been found in cells and certain proteins specifically bind to Z-DNA. In other work^{20, 29, 32}, the nomenclature L-DNA was used to describe a different form of left-handed DNA with a base-pair rise of 0.48 nm/bp and persistence length of 3-7nm^{29, 32}, values that varied significantly from the values for Z-DNA (0.37 nm/bp, and 200 nm, respectively). The estimated helix repeat of L-DNA is 13-16bp, resulting in an extension of 1.4 times B-DNA^{19-21, 29, 32-34}. The free energy difference between B-DNA and L-DNA is estimated to be ~2.5 k_BT per base pair, close to the free energy of melting (strand separation) which is ~2 k_BT for an AT base pair and ~3 k_BT for a GC base pair (from³⁵, based on random sequence), in line with the suggestion that left handed-DNA is partially torque-melted^{29, 32, 33}.

For better understanding, the DNA states at various regimes of force and torque are ordered in phase diagrams. Early theoretical suggestions pointed towards a phase diagram with two states, right-handed B-DNA and left-handed 'L-DNA' at a biologically relevant force regime (up to several piconewtons) and a wide range of negative supercoil densities³⁶. Later work suggested a much more complex phase diagram where pure states emerge only in a small part of the phase diagram and underwound DNA generally adopts a mixed state in which multiple DNA states co-exist^{37, 38}. Other recent theoretical work even suggest the existence of even more structures by

adding a left-handed version of P-DNA, called Q-DNA with a helicity of ~42bp per turn³².

Here we experimentally examine the phase diagram of negatively supercoiled DNA in a wide range of supercoil density, from the biologically relevant regime of $\sigma \approx -0.05$ to very strong underwinding of values down to $\sigma = -2.5$. Using magnetic tweezers, we control the applied stretching force and supercoil density on a single DNA molecule. First, we map the DNA length as a function of supercoiling, which already allows to classify a number of DNA phases. Second, combining fluorescence microscopy with the magnetic tweezers³⁹, we visualize the location of DNA plectonemes and fluorescently labelled proteins along the DNA as a function of negative supercoiling density to determine which structures are present in each phase. We thus provide an experimental phase diagram of negatively supercoiled DNA in the mapped region of negative supercoiling down to $\sigma = -2.5$ and applied stretching force up to 4.5pN. Our observations reveal the coexistence of negative plectonemes, multiple DNA bubbles and L-DNA.

Materials and methods

Magnetic tweezers

In magnetic tweezers⁴⁰, one monitors the end-to-end length of a single DNA molecule that can be twisted and pulled upon. A torsionally constrained 20,666 kilobase pair (kb) double-stranded DNA (dsDNA) molecule is tethered between a surface and a magnetic bead to which a force can be applied and which can be rotated by external magnets (see Figure 2A). One end of the DNA molecule is attached to a glass surface by multiple digoxigenin (DIG)-antidigoxigenin (anti-DIG) bonds. In some experiments, this end of the DNA was labelled with multiple Atto-555 molecules. The other end of the DNA has multiple biotin labels and is attached to a 1 μ m diameter streptavidin-coated superparamagnetic bead (New England BioLabs, S1420S). The experiment takes place in a squared glass capillary with an approximate volume of 25 μ l (Vitrotubes, 8270-050, 0.7x0.7x50mm inner diameter), coated with 0.1% polystyrene in toluene solution and subsequently activated with anti-DIG antibody. The surface is passivated by Bovine Serum Albumin (BSA) (New England Biolabs, B9001S), which is incubated for at least one hour at a concentration of 10 mg/ml. Buffer exchanges occur by placing the new buffer at the inlet of the capillary, and using a syringe pump at the outlet to remove the old solution to a waste container in a smooth and controlled way. The position of the bead is tracked using video microscopy at high accuracy (~5 nm) and speed (frame rate 74Hz). By placing external magnets close to the bead (two magnet cubes, separated by 1mm from each other; Supermagnete, W-05-N, 5mm, Neodymium), a stretching force is applied which can be regulated by the distance between the bead and the magnets. When a constant force is applied, the DNA extension is constant, apart from fluctuations due to Brownian motion. Upon rotating the magnets within the x-y plane, the magnetized bead follows this rotary motion and as a result the linking number of the attached dsDNA changes.

Thus, positive or negative coils are introduced in or removed from the dsDNA. A rotation curve is generated by plotting the extension of the DNA molecule against the number of applied magnet rotations (Figure 3). At any given magnet configuration, the overall linking number is conserved when the DNA is topologically constrained (i.e. not nicked).

Fluorescence spectroscopy

We image DNA molecules that are negatively supercoiled and pulled horizontally in the focal plane. First, a DNA molecule is rotated to the desired amount of supercoiling by turning the top magnets while the DNA molecule is in a vertical orientation (part A in Figure 2). Subsequently, a side magnet (Supermagnete, Q-10-04-02-G, 10x4x2mm, Neodymium, gold-plated) is brought into close contact with the capillary. After the desired stretching force is reached by the side magnet, the top magnets are removed and the entire DNA molecule now is pulled to the side (part B in Figure 2). By slightly tilting the surface, the tethered DNA molecule can be brought into perfect horizontal alignment, along the focal plane, independent of bead size. With a 532nm laser, entering into the capillary from below, fluorescent molecules can be excited. Two imaging modes were used: 1) visualization of twist-induced structures of the DNA itself, by fluorescently labelling of the DNA (*iii* in Figure 2), and 2) visualization of binding positions of fluorescently labelled RPA, proteins that bind to single-stranded DNA (*iv* in Figure 2). The DNA was labelled with Cy3 as described in Ref 39. The RPA was fluorescently labelled with Tag-RFP as discussed in Ref. 41.

In all experiments, we used a buffer consisting of 30 mM NaCl, 60 mM Tris-HCl pH 7.5 and 0.1 mM Ethylenediaminetetraacetic acid (EDTA). To reduce the effects of free radicals, the buffers were degassed before every experiment by placing them into a vacuum chamber for 15 minutes. In experiments using fluorescently labelled molecules, sticking, as well as nicking of the DNA was reduced by adding free-radical-scavengers to the measurement buffer (trolox, NPG, PCA and PCD prepared as described in Ref. 39).

Results

DNA extension classifies the DNA phases

The supercoil density σ is defined to be zero when B-DNA is in a rotationally relaxed state with its natural B-DNA twist of 1 right-handed helix per 10.4 bases. The supercoil density then is given by the number of applied magnet turns divided by the number of naturally occurring helices in the B-DNA molecule. A supercoil density of $\sigma = -1$ would thus involve enough negative turns to remove all helicity from the B-DNA backbone, and $\sigma = -2$ would be enough to form a 'mirror-image' DNA structure with 10.4 bases per negative helical turn. Similarly, the linking number $L_k = 0$ in the rotationally relaxed state, while L_k decreases with the number of negative turns applied.

At low force (below 0.6pN), the supercoiling density dependence of the DNA extension is well understood. The

maximum length of the DNA molecule occurs when σ is zero. When a low number of positive (negative) rotations is applied, the DNA becomes overwound (underwound) and twists, whereas beyond a certain buckling point⁴², extra turns are absorbed into plectonemes, which makes the DNA extension decrease rapidly. In this regime, the slope of the rotation curve (the σ dependence of the extension, as shown in Figure 3) is set by the size of these supercoils: Increasing the linking number by one full turn induces one supercoil and reduces the extension by the length of DNA absorbed in this supercoil. The build-up of twist is relatively low at these low forces and the DNA backbones approximately maintain their B-DNA helical form. At larger forces, above approximately 0.6pN, DNA starts to adopt other forms than B-DNA for negative σ . This state has been called 'melted-DNA'²⁹.

To characterize the poorly described physical properties of this melted DNA, we measured how the DNA extension depends on (extreme) negative supercoiling at a number of forces up to 4.5pN (shown in Figure 3). At 4.5pN, the DNA extension stays nearly constant down to $\sigma = -1.9$, where a sharp kink occurs and after which the DNA length decreases linearly until a second kink occurs near $\sigma \sim -2.2$. The data for forces 1.0-2.5pN show similar shapes, except that the region between $\sigma = 0$ and the first kink do not show a linear plateau, but instead a monotonous decrease in length. The supercoiling density at which the first sharp kink occurs changes slightly with increasing force, from $\sigma = -1.93$ (1pN) to -1.88 (4.5pN). The second kink occurs at increasingly negative supercoiling density, from $\sigma = -2.06$ (1pN) to -2.20 (4.5pN). In contrast to Ref. 29, we do not observe any hysteresis between the backward and the forward curves (two examples are shown at 2.5 and 1.0pN), which suggests that no complex irreversible second-order structures are formed.

We note that the sharp kink at $\sigma = -1.9$ occurs close to the value of $\sigma = -2$, the supercoil density of left-handed DNA that would mirror the well-known right-handed B-form of DNA. In resemblance with the low-force B-DNA buckling point near $\sigma = -0.02$ (for $F=0.6$ pN), the DNA extension decreases approximately linearly for every induced negative turn, from $\sigma \sim -1.9$ down to $\sigma \sim -2.2$. The slope of the rotation curves beyond the buckling point at $\sigma = -1.9$ are 5.5-6.8 nm/turn for the forces of 2-4.5pN (the extensions at the smaller forces are relatively less steep than the 60 nm/turn in B-DNA at 0.5pN. This suggests that plectonemes in the left-handed DNA are approximately ten times smaller than those in B-DNA, which gives a rough estimate of the persistence length to be on the order of 3-7nm (assuming factors like the electrostatic repulsion to be comparable), consistent with L-DNA and much smaller than the values for Z-DNA. For this reason, we will from now on use the term L-DNA when referring to this left-handed DNA phase. Consequently, (i) we identify the sharp kink with a buckling point, where plectonemic L-DNA starts to form for $\sigma < -1.9$, (ii) we suggest that a pure L-form likely occurs near $\sigma = -1.9$, and (iii) this suggests that the wide region between $\sigma = 0$ and $\sigma = -1.9$ thus likely contains a mixture of B-DNA and L-

DNA (possibly augmented with other DNA structures). This is schematically summarized in the phase diagram of Figure 4, where the blue and orange parts show the regions in which plectonemes are formed in B- and L-DNA, respectively.

We thus can verify various phases of negatively supercoiled DNA: The relaxed B-DNA state, where $\sigma \equiv 0$, is shown in green as state A in the diagram of Figure 4 (lower panel). The well-known region of plectoneme formation in pure B-DNA is drawn in blue as state B. The transition from B-DNA to L-DNA is drawn as a mixed state C which occurs in a very wide range of forces and negative supercoiling. At the buckling point near $\sigma = -1.9$, we assume that all DNA is in the L-DNA form, (black line between C and D), and the plectoneme formation in pure L-DNA form is denoted by the orange region D. When the linear decrease in the rotation curve ends (red line between D and E), another phase E may start. Region F (white) is a region where the DNA extension is too short for our experiments ($< 5\%$ of the B-DNA contour length). To further characterize the suggested phase diagram, in particular the transition from B- to L-DNA, we measured binding of *Za77*, a Z-DNA binding protein, and visualized plectoneme and bubble formation.

Plectonemic DNA state

To visualize plectonemes and other dense DNA structures, we imaged single DNA molecules after fluorescent labeling. At low force ($< 0.6\text{pN}$) and mild unwinding ($-1 \ll \sigma < 0$), we observed fluorescently intense DNA spots along the DNA (Figure 5B, $\sigma = -0.02$, $F = 0.2\text{pN}$, corresponding to the purple dot in Figure 5A). The high-intensity spots in this representative example were dynamic and showed diffusive behavior. In an experiment where DNA was negatively twisted to reduce its extension by 25% at 0.5pN stretching force, the diffusion coefficient of these dynamic spots was $0.4 \mu\text{m}^2/\text{s}$. This result for negatively supercoiled DNA at low force is very similar to a comparable report for the positively coiled DNA, especially when taking into account that lower salt concentrations increase the diffusion constant³⁹. Upon nicking, the high intensity regions disappear instantly (see **Error! Reference source not found.**B), leading to a homogeneous intensity for the fluorescent molecule of the original (uncoiled) DNA length. All these observations fit the physical picture of plectonemic B-DNA. Alternative DNA structures such as ssDNA blobs that could form through hydrogen-bond reorganization (for example, hairpins) would likely result in a much slower disappearance of the high intensity regions upon nicking. Furthermore, the single-strand binding protein RPA does not bind DNA at these conditions of low force and mild unwinding, as previously reported¹⁶. We thus conclude that the state of the DNA at low force ($< 0.6\text{pN}$) and mild unwinding ($-1 \ll \sigma < 0$) is plectonemic B-DNA.

We also visualized DNA at much stronger negative supercoiling. At $\sigma = -0.5$, i.e. about one negative applied turn per $\sim 21\text{bp}$, we explored the DNA structure at 1.5pN and 2.0pN . At 1.5pN , highly dynamic dense DNA regions are present along the DNA length (Figure 5C), consistent with the occurrence of plectonemes. Interestingly, at an only slightly

higher force of 2.0pN , the fluorescent images are almost featureless (Figure 5D), similar to torsionally unconstrained B-DNA, indicating the absence of highly dense DNA regions such as plectonemes.

As mentioned above, the sharp change in the slope of the rotation curve at $\sigma = -1.88$ at stretching force 2.0pN (Figure 3 and Figure 5E) seems to indicate a buckling point at the end of the B- to L-DNA transition. The first frame in Figure 5G shows a fluorescence image of the DNA right at this point. In contrast with the buckling point of B-DNA at low force and supercoiling (region B in the lower panel of Figure 4), which shows a fully homogeneous fluorescence intensity, we observe dense DNA regions that are localized and stationary, indicating some structural variation like supercoiling is present (Figure 5F). Upon nicking (**Error! Reference source not found.**), these high-intensity regions disappear, albeit somewhat slower than for the conventional plectonemes at small σ . Since the relatively long relaxation time could be due to two reasons (it takes longer to relax the much larger number of negative supercoils, or the DNA structure could be distinctly different from B-DNA plectonemes), it is hard to draw unequivocal conclusions. Applying more negative turns than $\sigma = -1.88$ leads to a shortening of the DNA, which coincides with an increase in the intensity of stationary DNA-dense regions.

The presence of dense DNA structures and the dynamics of these structures highly depend on force and supercoiling density. A comparison of data for various forces in the region beyond the buckling point, i.e., for $\sigma < -1.9$, is visualized in the left two panels of Figure 6A. Here, a relatively small increase in negative supercoiling density is seen to have a significant effect on the emergence of DNA-dense regions. At the high stretching force of 5.7pN , more negative supercoiling needs to be induced to generate the same amount of DNA-dense regions, compared to the experiments at 2.4pN stretching force. The right two panels of Figure 6A show the results at different forces for a supercoiling density of $\sigma = -1.5$ and -1 . It shows that lowering the force and increasing the supercoiling density have comparable effects on the appearance of DNA-dense regions. Figure 6B shows the dynamics of the high-intensity regions in the kymographs at a constant force of 1.5pN but varying supercoiling density. The top images show a raw fluorescence image. All kymographs were corrected for bleaching and background (see Ref. 39 for details). Without supercoiling, no dense regions are observed. With relatively low negative supercoiling, very dynamic regions appear. With increasing negative supercoiling, the intensity in the DNA-dense region increases, but the dynamics decreases. Figure 6C and D show the effect of force on the dense regions. Next to a decrease in DNA-dense regions, a higher force also decreases the dynamics of these regions. Figure 6E shows the fluctuations in DNA extension as a function of supercoiling density for 1.0 , 1.5 and 2.0pN stretching force. This result shows that the fluctuations decrease with increasing force. Furthermore, there appears to be a supercoiling density at which a maximum of the fluctuations occurs, which is force dependent, i.e. at higher force, the maximum occurs at stronger negative supercoiling.

As suggested recently³⁸, the supercoiling density dependent fluctuations likely stem from transitions between different DNA states where twist and writhe are interchanged.

Summing up, when no supercoiling is applied, no plectonemes occur. Mild supercoiling combined with mild stretching forces results in highly dynamic plectonemic structures in the DNA. Increasing negative supercoiling results into more dense structures that are more static (possibly plectonemes, perhaps other structures). Increasing the force lowers the fluctuations in DNA extension, and shifts the point of maximal length fluctuations (transitions between plectonemes and underwound B-DNA/overwound L-DNA by thermal fluctuations) towards stronger negative supercoiling.

DNA bubbles visualized by RPA binding

We use a single-stand-DNA binding protein to probe the presence of dehybridized single-stranded DNA (ssDNA) in the mixed phase of negatively supercoiled DNA. In cells, ssDNA is rapidly bound and stabilized by ssDNA-binding proteins (SSBs). This prevents ssDNA from hybridizing into secondary structures and avoids unwanted effects like digestion of the DNA by nucleases. The main eukaryotic SSB is replication protein A (RPA), which also stabilizes transiently forming bubbles of ssDNA⁴³. Here we measure RPA binding and we directly visualize the position of the fluorescently labelled RPA molecules on the DNA at varying forces and under (extreme) negative supercoiling.

Previous RPA-binding experiments under mild ($\sigma \geq -0.06$) negative supercoiling showed that RPA did not bind up to 0.5pN. In other words, no (transient) bubble formation occurred at these conditions. Under the same supercoiling density, but at slightly higher forces, measured from 0.5 to 0.75pN, (transient) bubble formation did occur¹⁶. In line with these conditions, we assembled our fluorescently labelled RPA at 0.9pN onto DNA with supercoiling density $\sigma = -0.25$ (Figure 7A). In this regime, the extension of supercoiled DNA is 35% of that of relaxed B-DNA. Similar to the previous results, RPA assembly increased the DNA extension, which can be interpreted as signaling the presence of DNA bubbles: RPA stabilizes such bubbles and newly incoming RPA wedges into RPA-stabilized bubbles, causing progressive unwinding which leads to the removal of negative plectonemes¹⁶. In contrast with the previous measurements¹⁶, the RPA-induced extension at $\sigma = -0.25$ increased only up to 90% of its relaxed bare DNA length, instead of 100%.

At a higher force of 1.5pN, assembly of RPA, by contrast, does not change the extension significantly with negative supercoiling down to $\sigma = -1.1$ (Figure 7B, panel 2-5). At even stronger negative supercoiling ($\sigma = -1.4$), the extension even decreases upon RPA addition (Figure 7B first panel).

At an increased force of 2pN, and mild supercoiling density ($\sigma = -0.25$), RPA assembly does not affect the DNA extension. Introducing stronger negative supercoiling results in a length decrease due to RPA binding (Figure 7C). Although these results are at first sight different from the previously reported results at lower force and supercoiling densities, similar

interpretation can be made: RPA stabilizes DNA bubbles and newly incoming RPA wedges into RPA stabilized bubbles, causing progressive unwinding. In the strong negative supercoiling regime ($\sigma < -1$), however, L-DNA is likely opened up instead of B-DNA. Reducing negative twist then has to be balanced by *increasing* negative writhe, in order to maintain the same linking number. Increasing the writhe, forming plectonemes, then leads to a *decrease* in the DNA extension.

The assembly locations of the fluorescently labelled RPA are shown in Figure 8. No kymographs are shown, since the assembled RPA did not show any dynamics in the binding locations. Results at a constant force of 1.5pN and varying supercoiling densities (Figure 8A) show RPA binding at multiple locations that are apparently distributed all along the DNA molecule. Experiments done at higher forces (Figure 8B, 2.5pN left panel and 2.0pN middle panel) show similar results. Repeated assembly on the same molecule, with increasing supercoiling density, is shown in Figure 8B, right panel (where in between the measurements RPA was removed by positive supercoiling combined with lowering the stretching force to 0.3pN as described in Ref. 16). Upon decreasing supercoiling density down to $\sigma = -1.0$, more RPA binds and the fluorescence intensity changes from a number of high intensity regions to a nearly uniform binding of RPA. Decreasing the supercoiling density even further reduces the uniformity in the RPA binding again.

The main conclusion from visualization of the fluorescently labelled RPA under different force and supercoiling density, is that RPA is found to bind to multiple positions along the molecule under all these varying conditions. These positions appeared to be at random locations along the DNA and the kymographs showed no dynamics in the location of the fluorescent spots along the DNA. A previous hypothesis of RPA binding to one (transient) bubble, which subsequently grows upon binding of additional molecules of RPA, thus turned out to be unjustified.

A quantitative analysis of the number of bound RPA molecules is shown in Supplementary Information 2. In general, tens to a few hundred of RPA molecules are assembled onto the DNA, depending on applied stretching force and supercoiling density. Although our precision in determining the exact number of bound RPA molecules is limited (on the order of tens of molecules), a trend can be deduced at low force. For the lower 1.5 pN stretching force, we can conclude that RPA binding increases with increasingly negative supercoiling density (going from supercoiling density $\sigma = -0.4$ to $\sigma = -1.27$). For a stretching force of 2.0pN, the data are limited by measurement errors, and we cannot draw any firm conclusions on the supercoiling-density-dependent assembly. However, data obtained at 2.5pN again show a most significant binding of RPA around $\sigma = -1$.

Before these measurements of the binding of fluorescently labelled RPA to negatively supercoiled DNA, one could expect, as reported¹⁶, that after the initiation of RPA binding to a first DNA bubble, the application of additional rotations would lead to further growth of this single RPA-stabilized bubble. However, we clearly see the

appearance of multiple bubbles along the DNA, and therefore we conclude that additional binding of RPA does not only occur at the initial RPA-stabilized bubble. Another interesting result is the RPA-binding effect on DNA length. At low force (0.9pN) and $\sigma = -0.25$, the DNA length first decreases due to plectoneme formation (bottom panel of Figure 7), and consecutive RPA binding induces a length increase, resulting in a DNA length close to the relaxed B-DNA molecule. The latter can be interpreted¹⁶ as RPA-induced stabilization of transiently formed bubbles which absorbs negative plectonemes and thus induces a length increase. At the same supercoiling density, but larger stretching force (2.5pN), i.e. in the regime where the DNA length is not reduced by plectonemes, RPA binding does not affect the DNA length much. At 1.5pN the DNA length initially increases due to RPA binding, but with stronger negative supercoiling, the DNA length starts to decrease. This suggests that RPA binds to (static) bubbles, increasing the persistence length and thus the total DNA length. The stronger the negative supercoiling, the higher the probability that RPA stabilizes transiently formed bubbles in L-DNA regions. Since our results suggest a concurrence of plectonemes, bubbles and L-DNA, removal of L-DNA could also induce plectonemes, thus inducing a length decrease.

L-DNA probed by protein Z α 77

To probe the presence of left-handed DNA, we have examined the binding of the protein Z α to DNA. Z α specifically binds to the “zigzag” sugar-phosphate backbone of Z-DNA⁴⁴. We used the 77 amino acids minimal core domain of Z α , Z α 77 (also known as Z α _{ADARI}^{45, 46}), which is sufficient to bind to Z-DNA. Upon flushing in Z α 77, no effect on the DNA length was observed for torsionally relaxed DNA. However, upon introducing the Z-DNA binding protein to negatively supercoiled DNA, we observed a change in DNA extension, which indicates binding. An example of a binding curve at 3pN and $\sigma = -1.8$ is shown in Figure 9A (bottom panel). These data were taken close to the buckling point that presumably marks the end of the B- to L-DNA transition. Flushing in 65nM Z α 77 resulted in a DNA length decrease. Figure 9B shows the effect of force on a Z α 77-binding-induced decrease in DNA length. In these experiments 200nM Z α 77 was flushed in at zero supercoiling. An increasing amount of negative supercoiling was introduced at a constant rate of 10Hz magnet rotations (-0.005 σ /s) (black curve). The DNA end-to-end length was seen to decrease for increasingly negative σ . Rotating back with the same speed (red curve) resulted in some hysteresis, a further indication that Z α 77 was bound to the DNA. Interestingly, at lower forces, the backward traces had an increased extension, where at the higher forces the backward traces had a decreased length. The different force measurements were done on different molecules to ensure bare DNA starting positions.

Comparing the rotation curves of bare DNA with the forward (i.e. σ decreasing from 0 to -1.5) trace in the presence of Z α 77 at different forces (Figure 9C) shows a negligible effect on the DNA length at 1.5pN. The higher forces of 2.0 and 2.9pN show an increasing DNA length change in the presence of Z α 77 with

more negative supercoiling. A more detailed overview of the force dependence of the length change at $\sigma = -0.5$, $\sigma = -1.0$ and $\sigma = -1.5$ is shown in Figure 9D, which clearly shows that stronger negative supercoiling leads to a larger DNA length decrease, in particular near an applied force of 2.5pN. We did fluorescently label the Z α 77 protein for visualization experiments, but when used at 65nM, the fluorescent background due to proteins that were unspecifically bound to the surface was too high to permit detection of the protein on DNA.

Z α 77 binding thus has a force- and supercoiling-density-dependent effect on the DNA length change. As with every DNA-binding protein, we cannot exclude that binding of Z- α 77 has an effect on the DNA structure. A possible explanation for the DNA length changes that we observe is stabilization of the left-handed DNA structure due to Z α 77 binding. When the left-handed structure is stabilized by the protein, this part of the DNA is not capable of torque absorption by extra twist in the backbones. Instead of negative-supercoil absorption in twist, more DNA bubbles or plectonemes then have to be formed, depending on the applied stretching force. The plausibility of this model is shown by a calculation in Supplementary Information 3. The Z α 77 binding data suggests a larger occurrence of L-DNA at more strongly negative supercoiled DNA, especially around an applied stretching force of 2.5pN at $\sigma \leq -1$.

Discussion and conclusion

Based on the DNA extension, we have obtained a phase diagram of negatively supercoiled DNA with the following phases: relaxed B-DNA when $\sigma = 0$, plectoneme formation in pure B-DNA at forces below 0.6pN and mild negative supercoiling, a transition from B-DNA to L-DNA with decreasing σ down to -1.90 ± 0.03 , followed by plectonemic L-DNA for σ values down to -2.11 ± 0.09 . The start of the plectonemic L-DNA gives an upper limit on the estimated helicity of L-DNA, since the plectonemic L-DNA only starts after the pure L-DNA absorbed the maximum supercoiling in twist, i.e. before it is energetically more favorable to absorb the extra induced negative supercoiling in writhe. The found helicity of pure L-DNA (12bp/turn) is in good agreement with previous torque measurements (~ 13 bp/turn²⁹). We note that constructing a phase diagram based merely on force-extension curves can be ambiguous, since phases may mix in such a way that a phase transition does not appear unambiguously from extension data (as happens, for example, for the B to supercoiled-P transition in the positive supercoiling density regime at forces around 10pN³²). However, in the low-stretching-force regime we explored in this study, the plectonemic L-DNA starts after a pronounced buckling point, allowing for precise determination of the phase transition. Analogous to P-DNA in the positive supercoiling regime, it has been suggested that Q-DNA exists in the negative supercoiling regime with a helicity of ~ 42 bp per negative turn³². One might speculate that the ‘unknown’ phase transition appearing in our diagram could be a transition from plectonemic L-DNA to

plectonemic Q-DNA, but we currently have no experimental evidence for that.

Our results for both the helicity (12bp/turn) and persistence length (~5nm) of L-DNA are in good agreement with previous reports. Our experiments with fluorescently labelled RPA allow commenting on the mixed-phase. As we saw, some RPA-bound (transient) bubbles do occur in L-DNA. The decrease in extension upon RPA binding, however, suggests that L-DNA was opened up in order to allow RPA binding, inducing plectonemes into the L-DNA and thus decreasing the length, a similar mechanism as the one proposed for RPA binding to B-DNA¹⁶. The observation that, close to the buckling point, RPA only sparsely binds to L-DNA, even actively opening up the DNA, suggests that, most likely, L-DNA is the pure DNA form just before the buckling point. The fact that RPA is able to open up L-DNA, supports the estimate of similar free energies for dehybridization of L-DNA and B-DNA. Our low-force estimate for the helical pitch of L-DNA is 12bp, where Ref. 29 reported a helical repeat starting at ~12bp at low force and increasing to 15bp at 36pN. Since force-induced stretching of DNA has been reported to have an increasing effect on helicity⁴⁷, we believe 12bp/turn is the best estimate for the helicity of L-DNA. Finally we note that this is the same value as the helicity of Z-DNA¹³. At low supercoiling density and fairly low force (≤ 2 pN), the observed DNA-dense regions are highly dynamic, and consistent with plectoneme formation. Upon going to stronger negative supercoiling, the DNA-dense regions become less dynamic. Based on the fluorescence intensity profile, it is hard to distinguish between plectonemes and local blobs with large ssDNA secondary structures. Highly dynamic structures are most likely plectonemes. Non-dynamic structures, however, do not necessarily exclude plectonemes, since plectonemes could be trapped at certain regions.

In conclusion, we have classified DNA phases based on DNA length as a function of supercoiling. Direct visualization of DNA-dense regions, DNA bubbles formation and $Z\alpha 77$ binding reveals plectoneme dynamics together with the appearance of multiple bubbles and left-handed DNA. The transition from B-DNA to L-DNA shows a complex interplay between multiple DNA conformations. The concurrence of these multiple conformations at biologically relevant conditions could play an important role in the recruitment and functioning of DNA-binding proteins.

Acknowledgements

We would like to thank Jaco van der Torre for making the DNA constructs and Jacob Kerssemakers for discussions. This work was supported by the Netherlands Organisation for Scientific Research (NWO/OCW), the Foundation for Fundamental Research on Matter (FOM; to R.V., C.D.), the European Research Council for ERC Advanced Grant NanoForBio (to C.D.), and the French National Research Agency (ANR) and by the A*MIDEX project (n° ANR-11-IDEX-0001-02) funded by the «Investissements d'Avenir» French Government program (to M.M.).

Notes and references

^a Department of Bionanoscience, Kavli Institute of Nanoscience, Delft University of Technology, Lorentzweg 1, 2628 CJ Delft, the Netherlands.

^b Centre de Recherche en Cancérologie de Marseille; CNRS UMR7258; Inserm U1068; Institut Paoli-Calmettes; Aix-Marseille Université, 27 Bd Leï Roure, BP 30059, 13273 Marseille Cedex 09, France.

* Equal contribution.

** Email: C.Dekker@tudelft.nl.

Electronic Supplementary Information (ESI) available: [Supplemental Figure 1]. See DOI: 10.1039/b000000x/

- R. Wing, H. Drew, T. Takano, C. Broka, S. Tanaka, K. Itakura and R. E. Dickerson, *Nature*, 1980, **287**, 755-758.
- K. Havas, A. Flaus, M. Phelan, R. Kingston, P. A. Wade, D. M. Lilley and T. Owen-Hughes, *Cell*, 2000, **103**, 1133-1142.
- L. Postow, N. J. Crisona, B. J. Peter, C. D. Hardy and N. R. Cozzarelli, *Proceedings of the National Academy of Sciences of the United States of America*, 2001, **98**, 8219-8226.
- C. Bustamante, Z. Bryant and S. B. Smith, *Nature*, 2003, **421**, 423-427.
- L. F. Liu and J. C. Wang, *Proceedings of the National Academy of Sciences of the United States of America*, 1987, **84**, 7024-7027.
- F. Kouzine, A. Gupta, L. Baranello, D. Wojtowicz, K. Ben-Aissa, J. Liu, T. M. Przytycka and D. Levens, *Nature structural & molecular biology*, 2013, **20**, 396-403.
- M. Petersheim and D. H. Turner, *Biochemistry*, 1983, **22**, 256-263.
- P. Yakovchuk, E. Protozanova and M. D. Frank-Kamenetskii, *Nucleic acids research*, 2006, **34**, 564-574.
- J. Marmur and P. Doty, *Journal of molecular biology*, 1962, **5**, 109-118.
- J. H. Jeon and W. Sung, *Biophysical journal*, 2008, **95**, 3600-3605.
- A. H. Wang, G. J. Quigley, F. J. Kolpak, J. L. Crawford, J. H. van Boom, G. van der Marel and A. Rich, *Nature*, 1979, **282**, 680-686.
- A. Rich, A. Nordheim and A. H. Wang, *Annual review of biochemistry*, 1984, **53**, 791-846.
- T. J. Thomas and V. A. Bloomfield, *Nucleic acids research*, 1983, **11**, 1919-1930.
- F. Kouzine and D. Levens, *Frontiers in bioscience : a journal and virtual library*, 2007, **12**, 4409-4423.
- C. Naughton, N. Avlonitis, S. Corless, J. G. Prendergast, I. K. Mati, P. P. Eijk, S. L. Cockcroft, M. Bradley, B. Ylstra and N. Gilbert, *Nature structural & molecular biology*, 2013, **20**, 387-395.
- I. De Vlaminck, I. Vidic, M. T. van Loenhout, R. Kanaar, J. H. Lebbink and C. Dekker, *Nucleic acids research*, 2010, **38**, 4133-4142.
- S. B. Smith, Y. Cui and C. Bustamante, *Science*, 1996, **271**, 795-799.
- P. Cluzel, A. Lebrun, C. Heller, R. Lavery, J. L. Viovy, D. Chatenay and F. Caron, *Science*, 1996, **271**, 792-794.
- A. Sarkar, J. F. Leger, D. Chatenay and J. F. Marko, *Physical review. E, Statistical, nonlinear, and soft matter physics*, 2001, **63**, 051903.
- Z. Bryant, M. D. Stone, J. Gore, S. B. Smith, N. R. Cozzarelli and C. Bustamante, *Nature*, 2003, **424**, 338-341.
- J. Leger, G. Romano, A. Sarkar, J. Robert, L. Bourdieu, D. Chatenay and J. Marko, *Physical review letters*, 1999, **83**, 1066.
- J. F. Allemand, D. Bensimon, R. Lavery and V. Croquette, *Proceedings of the National Academy of Sciences of the United States of America*, 1998, **95**, 14152-14157.
- T. R. Strick, J. F. Allemand, D. Bensimon and V. Croquette, *Biophysical journal*, 1998, **74**, 2016-2028.
- J. Wereszczynski and I. Andricioaei, *Proceedings of the National Academy of Sciences of the United States of America*, 2006, **103**, 16200-16205.

25. T. R. Strick, J. F. Allemand, D. Bensimon, A. Bensimon and V. Croquette, *Science*, 1996, **271**, 1835-1837.
26. S. A. Harris, C. A. Laughton and T. B. Liverpool, *Nucleic acids research*, 2008, **36**, 21-29.
27. T. Lionnet, S. Joubaud, R. Lavery, D. Bensimon and V. Croquette, *Physical review letters*, 2006, **96**, 178102.
28. G. L. Randall, L. Zechiedrich and B. M. Pettitt, *Nucleic acids research*, 2009, **37**, 5568-5577.
29. M. Y. Sheinin, S. Forth, J. F. Marko and M. D. Wang, *Physical review letters*, 2011, **107**, 108102.
30. F. C. Oberstrass, L. E. Fernandes and Z. Bryant, *P Natl Acad Sci USA*, 2012, **109**, 6106-6111.
31. A. Rich and S. Zhang, *Nature reviews. Genetics*, 2003, **4**, 566-572.
32. J. F. Marko and S. Neukirch, *Physical Review E*, 2013, **88**, 062722.
33. F. C. Oberstrass, L. E. Fernandes and Z. Bryant, *Proceedings of the National Academy of Sciences of the United States of America*, 2012, **109**, 6106-6111.
34. M. Lee, S. H. Kim and S. C. Hong, *Proceedings of the National Academy of Sciences of the United States of America*, 2010, **107**, 4985-4990.
35. J. SantaLucia, Jr., *Proceedings of the National Academy of Sciences of the United States of America*, 1998, **95**, 1460-1465.
36. A. Sarkar, J. F. Leger, D. Chatenay and J. F. Marko, *Phys Rev E*, 2001, **63**.
37. J. F. Marko and S. Neukirch, *Physical review. E, Statistical, nonlinear, and soft matter physics*, 2013, **88**, 062722.
38. H. Meng, J. Bosman, T. van der Heijden and J. van Noort, *Biophysical journal*, 2014, **106**, 1174-1181.
39. M. T. van Loenhout, M. V. de Grunt and C. Dekker, *Science*, 2012, **338**, 94-97.
40. I. Vilfan, J. Lipfert, D. Koster, S. Lemay and N. Dekker, in *Handbook of Single-Molecule Biophysics*, Springer, 2009, pp. 371-395.
41. M. Modesti, *Methods in molecular biology*, 2011, **783**, 101-120.
42. S. Forth, C. Deufel, M. Y. Sheinin, B. Daniels, J. P. Sethna and M. D. Wang, *Physical review letters*, 2008, **100**, 148301.
43. C. Iftode, Y. Daniely and J. A. Borowiec, *Critical reviews in biochemistry and molecular biology*, 1999, **34**, 141-180.
44. H. S. Chung and W. A. Eaton, *Nature*, 2013, **502**, 685-688.
45. A. Y. Lushnikov, B. A. Brown, 2nd, E. A. Oussatcheva, V. N. Potaman, R. R. Sinden and Y. L. Lyubchenko, *Nucleic acids research*, 2004, **32**, 4704-4712.
46. T. Schwartz, K. Lowenhaupt, Y. G. Kim, L. Li, B. A. Brown, 2nd, A. Herbert and A. Rich, *The Journal of biological chemistry*, 1999, **274**, 2899-2906.
47. J. Gore, Z. Bryant, M. Nollmann, M. U. Le, N. R. Cozzarelli and C. Bustamante, *Nature*, 2006, **442**, 836-839.

ARTICLE

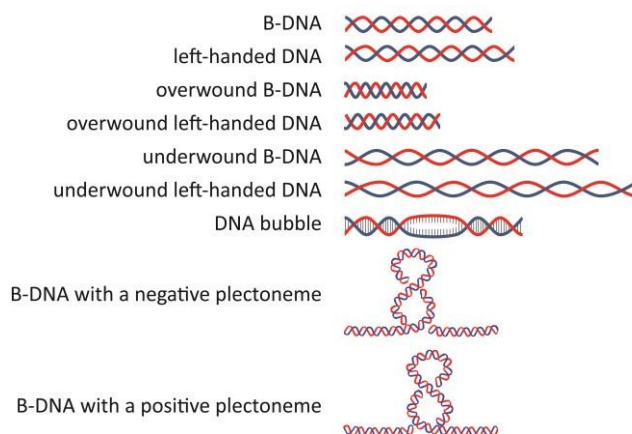


Figure 1: Various DNA configurations. The most common form of naturally occurring DNA is the double-stranded (dsDNA) B-form, where, without the application of stretching force or torque, the DNA backbone makes a right-handed helical turn with a repeat of 10.4bp (with a length of 3.5nm for 1 turn along the molecule)¹. Left-handed DNA is also discussed to occur *in vivo*³¹. Two different forms have been discussed: Z-DNA, with a well-defined 12bp helical left-handed helical turn (1 turn = 4.4nm long)¹³, and L-DNA with 12-15 bp per helical turn (1 turn = 6-7nm long)²⁹. Under the influence of positive torque, B-DNA can take up more coils per turn (overwound B-DNA), while left-handed DNA becomes underwound. Negative torque will underwind B-DNA and overwind left-handed DNA. Under certain underwinding conditions, double-stranded B-DNA can open up to form a 'bubble'. Instead of twisting and thus changing the number of base pairs per turn, rotations can also be absorbed by plectoneme formation, see the two bottom panels.

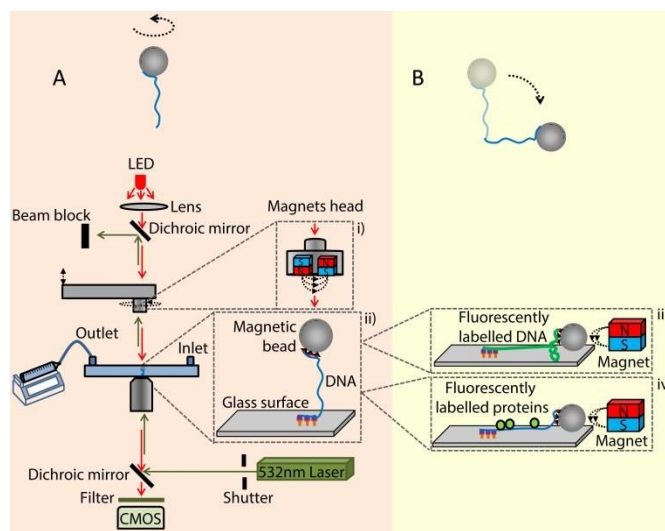


Figure 2: Single-molecule magnetic tweezers (side view in x-z plane). (A) Vertical DNA alignment. The lower inset *ii*) shows how an individual double-stranded DNA (dsDNA) molecule with DIG-labels is tethered to an anti-DIG antibody-coated glass surface of a glass capillary. The other end of the DNA has multiple biotin-labels which bind to a streptavidin-coated bead. Above the capillary, a magnet holder containing two magnets is placed (inset *i*). The magnets apply a stretching force that can be adjusted by changing the height with the motor stage. When rotating the magnets within the x-y plane, the bead follows these rotations and torque is applied onto the molecule. Red LED light is made parallel by a lens and illuminates the beads. A CMOS camera records the bead images. Buffers containing beads, proteins, etc., can be inserted into the capillary by pipetting it into the inlet. By turning on the syringe pump, new buffer is sucked into the capillary. (B) Horizontal DNA alignment allows for simultaneous fluorescence spectroscopy. Compared with A), the magnet head depicted in *i*) is now moved away, while keeping the magnetic bead rotationally clamped, and a side magnet is added to pull the molecule sideward, as shown in *iii*) and *iv*). A 532nm laser excites fluorescent molecules. Labelling the DNA allows visualization of the DNA structure (*iii*), while fluorescently labelled proteins allow determination of the protein-binding position (*iv*).

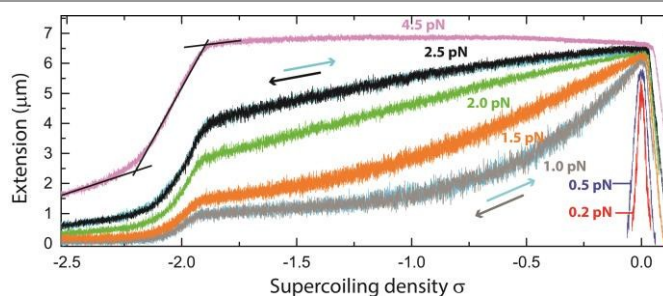


Figure 3: Rotation curves of DNA at applied forces between 0.2 and 4.5 pN. The data show the DNA extension (μm) as a function of the supercoiling density σ for a 20,666 bp dsDNA. The torsionally relaxed state of B-DNA is defined to have supercoiling density 0. At 1.0 and 2.5 pN the overlapping forward (respectively grey and black) and backward (light blue) trace show the absence of hysteresis. The black lines on the curve at 4.5 pN show how the buckling points are determined.

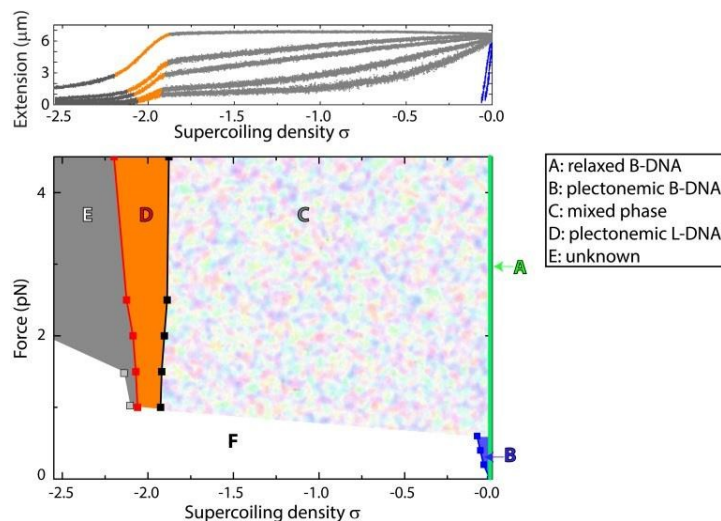


Figure 4: Lower panel: Phase diagram of DNA as a function of negative supercoiling density σ and applied stretching force (pN). For relaxed B-DNA, $\sigma \equiv 0$ (phase 'A'). Below 0.6 pN and at negative σ , plectonemic B-DNA is formed. Phase 'B' represents a coexistence of plectonemic and regular B DNA. Above 0.6 pN, a phase 'C' occurs which is a mixture of DNA with different helicities. Due to the transition from B- to L-DNA, there is a coexistence of (plectonemic) B-DNA, DNA bubbles, and (plectonemic) L-DNA. Phase 'D', between $\sigma = -1.9$ and $\sigma = -2.1/-2.2$, is a coexistence between regular and plectonemic L-DNA. At $\sigma < -2.1/-2.2$ an unknown phase starts ('E'). F is a region that cannot be experimentally measured, because the DNA extension is shorter than 5% of the contour length. Top panel shows the rotation curves of 20,666 bp dsDNA at forces between 0.2 and 4.5 pN (same data as the rotation curves in Figure 3).

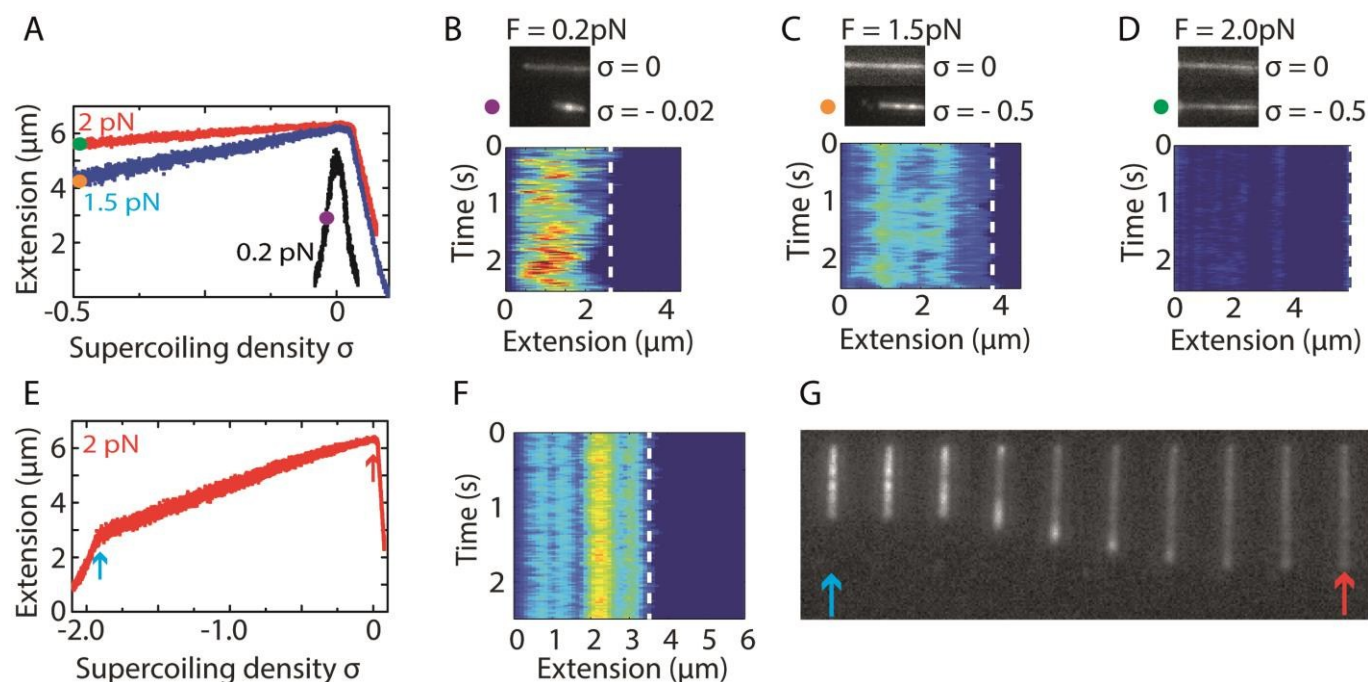


Figure 5: Pletoneme formation and dynamics are force and supercoiling dependent. (A) Rotation curves at 0.2, 1.5 and 2pN indicate the conditions of data in figures B), C) and D). (B) Top panel shows an image of fluorescently labelled DNA at $\sigma = 0$ and $\sigma = -0.02$ at stretching force of 0.2pN. Lower panel shows the kymograph of the DNA fluorescence patterns at $\sigma = -0.02$. The kymograph was corrected for bleaching and background, i.e. the homogeneous B-DNA intensity for non-supercoiled DNA is removed and only additional (pletonemic) DNA is visible (see ³⁹ for details). (C), (D) similar to B), but at $\sigma = -0.5$ and 1.5pN and 2pN, respectively. (E) Rotation curve at 2pN between $\sigma = -2$ and 0. At $\sigma \approx -1.88$ the buckling point marks the end of the transition from B- to L-DNA. (F) High-intensity regions in the DNA at $\sigma = -1.88$ show the absence of significant dynamics. (G) Upon nicking of the molecule shown in F), the molecule relaxes: the high-intensity regions move towards the ends and gradually disappear. Total duration from left to right is 180 ms (images taken at 50 Hz). All kymographs have the same color scale.

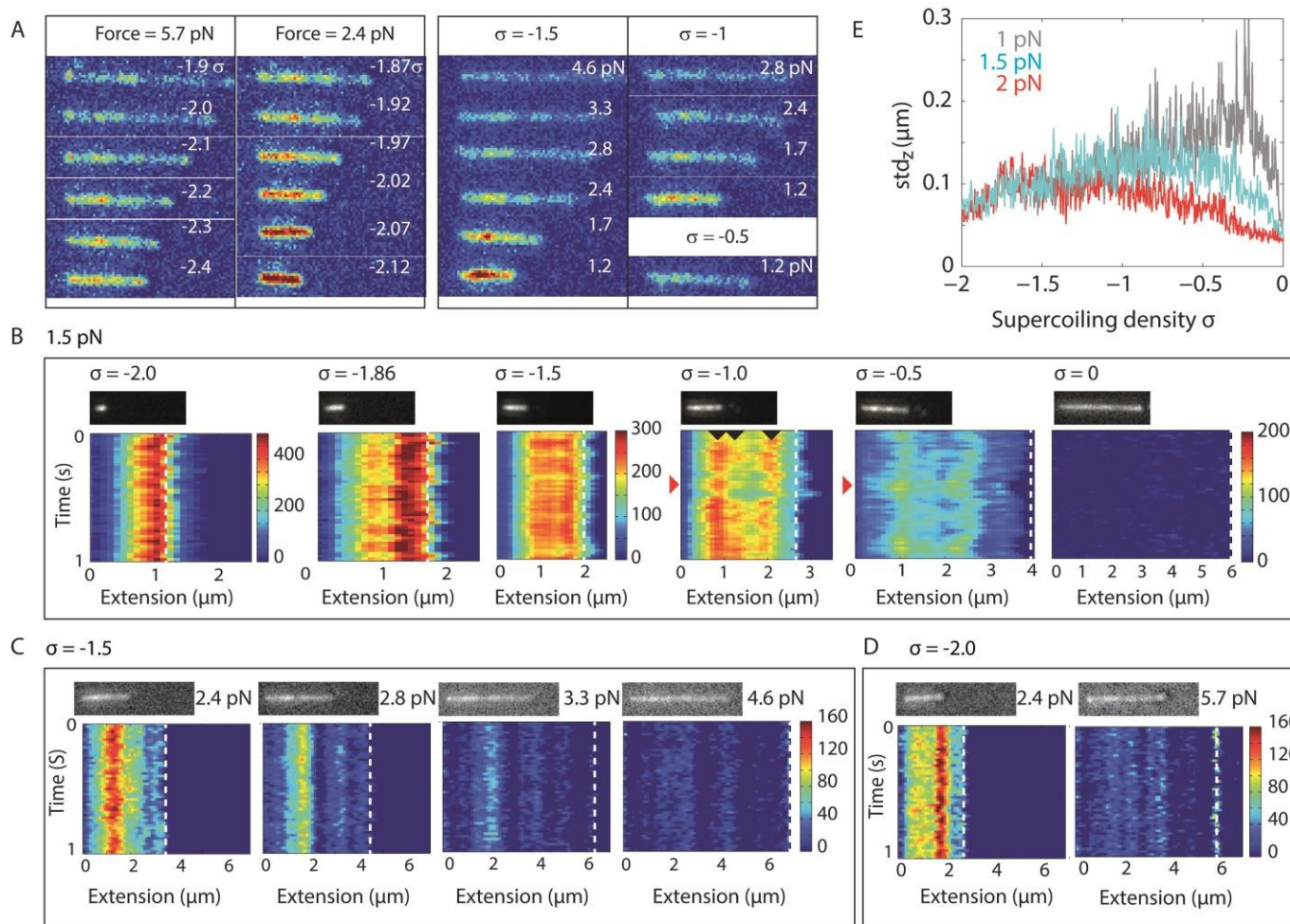


Figure 6: (A) Examples of DNA structures at various supercoiling densities and forces. All images are shown on the same colour scale. (B-D) Dynamics of DNA at various force and supercoiling densities as shown by fluorescent intensity fluctuations. (B) Kymographs of the DNA fluorescence patterns at 1.5 pN and σ from 0 to -2. While at $\sigma = -0.5$, highly dynamic DNA intensities are observed, DNA structures appear rather stationary and condensed at $\sigma = -1.5$ (regime C in Figure 4) and $\sigma = -2$ (regime D in Figure 4). DNA length decreases as intense DNA regions appear (see panel B, kymographs $\sigma = -0.5$ and 1 at time points shown by red arrows). DNA structures that show significant dynamics at $\sigma = -0.5$, localize to several areas at $\sigma = -1$, as depicted by black arrows. These areas merge upon increasing negative supercoiling (see the kymographs at $\sigma = -1.5$ and -1.86). In panels C and D, higher forces were applied to the stationary DNA structures at $\sigma = -1.5$ and $\sigma = -2$, to see how the contrast changes with force. (E) DNA length fluctuations as quantified by calculating the standard deviation of the DNA extension. The size of the sampling window for the standard deviation was 10 data points. All images were corrected for bleaching and background (see Ref. 31 for details). We show sample time windows of 1 second, which is characteristic to represent the dynamics at this regime. The images are representative of at least three measurements per condition.

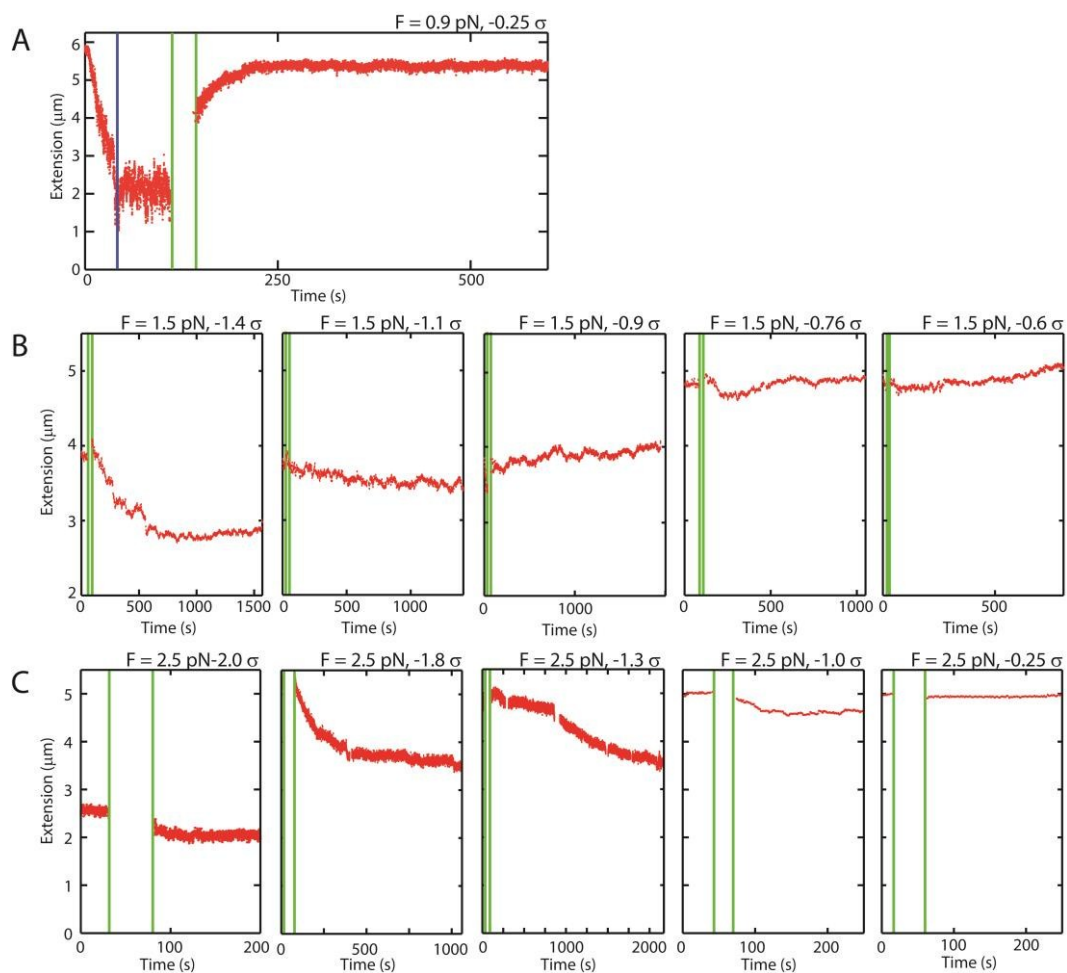


Figure 7: Assembly traces of RPA at A: 0.9 pN, B: 1.5 pN, and C: 2.5pN. Each trace is from a separate experiment with a different capillary and molecule. Green lines mark the start and end of the period of flushing in RPA. Red trace is a 100-point moving average of the extension as function of time. (A) In the first 50s (blue line), B-DNA is brought from $\sigma = 0$ to $\sigma = -0.25$ under 0.9pN stretching force. At $t = 110$ s, RPA is flushed in, after which a length increase is observed, bringing the final length close to the length of relaxed B-DNA. (B),(C) Effect of RPA binding at a stretching force of 1.5pN (B), or 2.5pN (C). Before $t = 0$, the molecule is brought to the indicated supercoiling densities.

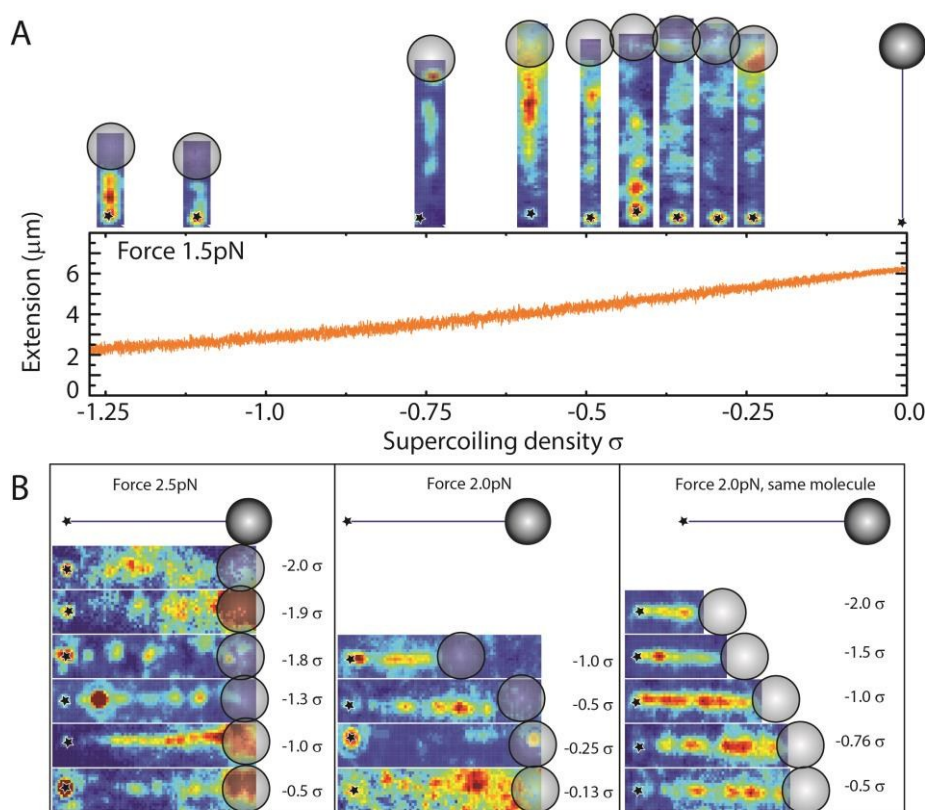


Figure 8: Visualization of RPA binding. The attachment point of the DNA to the glass surface is fluorescently labelled, and indicated by a star in the images. To illustrate the bead location, a bead image is overlapping the fluorescence image. (A) At a constant force of 1.5 pN, the binding of fluorescently labelled RPA is imaged at varying supercoiling densities. As a reference, the rotation curve showing the extension dependence of σ is shown in the lower panel. (B) Visualization of RPA binding at 2.5 (left panel) and 2.0 pN (middle and right panel). All data is acquired using new molecules for each experiment, except for the results shown in the right panel. For the later images, after visualization of the RPA, the molecule was rotated to positive supercoiling and the force was consecutively lowered to 0.3 pN (i.e. conditions known to disassemble RPA¹⁶), before RPA was assembled again at stronger negative supercoiling than the previous measurement. Independent of stretching force and supercoiling density, RPA is observed to be bound at multiple locations along the molecule. The color scale is optimized for identification of binding position.

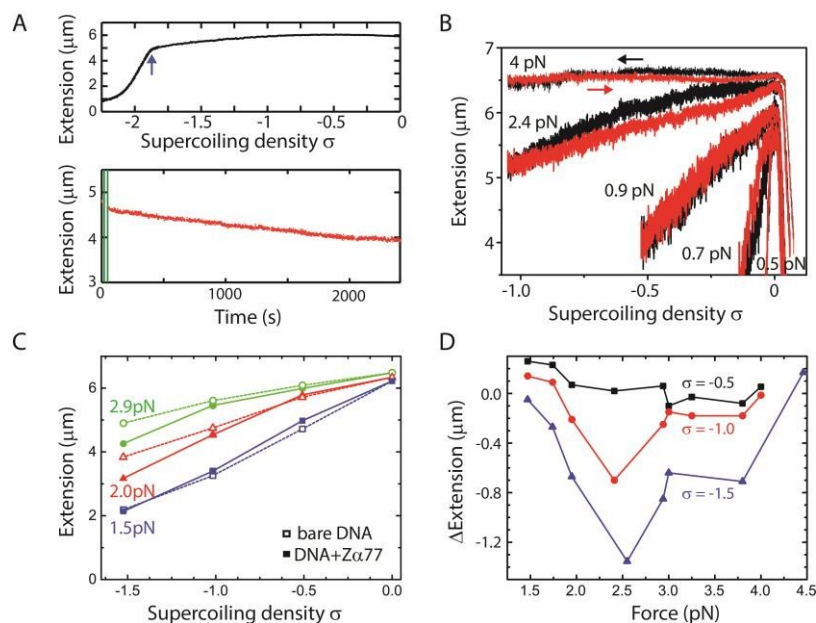


Figure 9: Z α 77 binding to negatively supercoiled DNA. (A) Top panel: Rotation curve of bare DNA at 3 pN. The arrow indicates $\sigma = -1.8$. Lower panel: Z α 77 binding curve. Upon flushing in 65 nM of Z α 77 at $\sigma = -1.8$ and stretching force 3 pN, the DNA extension decreases. (B) At different forces (with a new molecule for every force)

Z α 77 was flushed in when the DNA molecule was in a torsionally relaxed state. In the presence of unbound proteins, an increasing amount of negative supercoiling was induced (black curve) with a magnet rotation speed of 0.005 σ /s. The backward trace (red) showed hysteresis upon reducing the induced negative supercoiling, an indication that Z α 77 was bound to the DNA molecule. (C) The extension of bare DNA in the absence of proteins (solid line and solid data points) compared with the forward trace (increasing the amount of negative supercoiling) in the presence of Z α 77 proteins (dashed line, open data points). A concentration of 200nM Z α 77 was flushed in when the DNA was in a torsional relaxed state and the increasing negative supercoiling was induced subsequently. (D) Force-dependent difference between bare DNA and DNA with Z α 77 bound, measured such as in C, with $\sigma = -0.5$ (black), $\sigma = -1.0$ (red) and $\sigma = -1.5$ (blue).
